Stability Analysis of an Ultrasonic Motor for a new wave amplitude control

Frédéric Giraud, Betty Lemaire-Semail
Laboratory of electrotechnics and power electronics of Lille
Avenue Paul Langevin
59655 Villeneuve d'Ascq Cedex
Email: first name.name@polytech-Lille.fr

Julien Aragones, Jacques Robineau
Jean-Thierry Audren
SAGEM SA defence and security
Le Ponant de Paris
27 rue Leblanc
75512 Paris Cedex 15, France

***Abstract*—Using Piezo electric actuators can reduce bulk size of servomechanisms; they are thus very interesting in avionics applications. But mechanical overload on shaft of a Traveling Wave Ultrasonic Motor often results in a sudden stop and stalling of the motor. To avoid this drawback, one can increase the supply voltage or add a control loop in the rotating reference frame of the traveling wave. The consequences are extra power losses or lower dynamic performances.**

The proposed method takes advantage of classical control and in a rotating frame one : stability and dynamic performances are obtained at low supply voltage level. Experimental runs are presented.

I. Introduction

Traveling wave Ultrasonic Motors (TWUM) exploit a piezoelectrically generated flexural wave which propagates at the surface of a stator. This wave is able to propel by contact a rotor strongly pressed on it. Friction produced by the contact mechanism is at the origin of numerous advantages, among which we can find: braking without supply, a high torque to mass ratio and high torque - low speed characteristics. Thus, while a speed reducer is often needed with an electromagnetic motor, it becomes useless in applications using TWUM: this leads to lightweight and compact applications. These features really increase the interest of avionics industry for these motors for servo applications. Unfortunately, they are very difficult to control. First, and because torque generation is non linear, it is difficult to precisely drive a load. However, solutions have been provided to solve that problem [1] and achieve precise position control in optoelectronic applications[2]. Secondly, the resonant behavior of the stator is very sensitive to the external conditions: temperature, load torque or mounting conditions. For example, the motor may stall if a mechanical overload is applied on the shaft, and this is seriously decreasing the reliability of servo mechanisms actuated by TWUM. Reducing motor's sensitivity to external torque variations is thus a key issue to use them in avionic applications. In fact, bumps are typical of this kind of environment and random disturbances are applied on the the load while high accuracy of position or speed control is needed. To solve this problem, one can increase the supply voltage. This puts off the torque limit which makes the motor stalling, but does not remove the problem completely. Moreover, it increases the power losses and thus decreases the efficiency of the motor. Other solutions are proposed in [3][4]; [4] is based on the control of the motor in a rotating reference frame fixed to the traveling wave. By controlling the phase shift between the supply voltage and the traveling wave, it is possible to ensure operation for any load conditions. However, this solution slows down the traveling wave's dynamic. When implemented in a position control, this leads to lower dynamic performances compared to classical frequency control. This article aims at describing a new control method which helps to improve reliability of the motor's operation at low supply voltage level although keeping good dynamic performances during transitory operations. For that purpose, an overview of modeling of these motors is given. Then the proposed control is detailed. Experimental results are given in the final section for an industrial optoelectronic application

II. Modelling overview

A. Modelling in the $\alpha\beta$ frame.

A TWUM is made of a ring shaped stator on which piezoelectric elements are bonded. If these elements are supplied close to the resonant frequency of this mechanical set, a bending wave is propagating in the stator. This travelling wave is able to propel by friction a rotor pressed on it (figure 1).

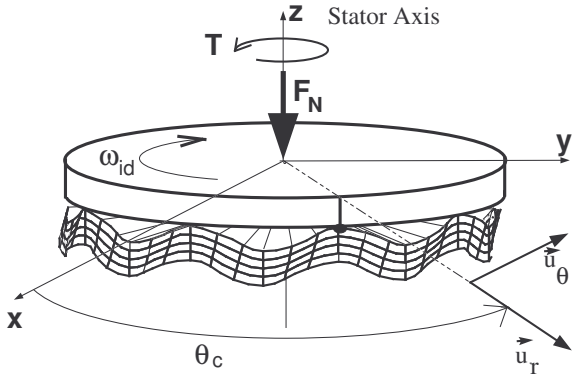

Fig. 1. Vibrating stator and the rotor pressed on it.

Some authors [5][6] describe the energy conversion process for TWUM. This process can be divided into three stages. In

the first stage, the supply voltages named v_α and v_β create forces by the inverse piezoelectric effect. In the second stage, the stator is vibrating because of these forces. The deformation w along z axis can be written as 1

$$w(\theta,t) = w_\alpha(t)\cos(\theta) + w_\beta(t)\sin(\theta) \tag{1}$$

w_α and w_β are the stationary wave's amplitude, which occur if v_α and v_β are supplied alone respectively, and k is the mode number. In fig 1 the stator is in contact with the rotor at one contact point along the wavelength. The wave crest location θ_c can be deduced from w_α and w_β by[7]:

$$k\theta_c = tan^{-1}\frac{w_\beta}{w_\alpha} \tag{2}$$

The relationship between w_α , w_β and v_α ,v_β is a 2nd order type equation

$$m\ddot{w}_\alpha + d_s\dot{w}_\alpha + cw_\alpha = Nv_\alpha - f_{r\alpha} \tag{3}$$

$$m\ddot{w}_\beta + d_s\dot{w}_\beta + cw_\beta = Nv_\beta - f_{r\beta} \tag{4}$$

m,c, d_s and N are parameters of the stator; [7]and [8] describe the protocol to identify these parameters. The resonant frequency of the stator is given by $\omega_0 = \sqrt{\frac{c}{m}}$.

In equation 3, $f_{r\alpha}$ and $f_{r\beta}$ are taking into account the external forces acting on the stator which are:

- the normal force pressing the rotor on the stator F_N
- the load torque T

Under ideal contact assumption (no sliding and ideal punctual contact condition) , it is possible to give a relationship between $f_{r\alpha}$, $f_{r\beta}$, F_N, and T:

$$\begin{pmatrix} f_{r\alpha} \\ f_{r\beta} \end{pmatrix} = R(k\theta_c)\begin{pmatrix} F_N \\ k\frac{h}{b^2}T \end{pmatrix} \tag{5}$$

h is stator's thickness and b is stator's radius, and depend on motor's geometry. $R(k\theta_c)$ is the well known rotational matrix, already used in electromagnetic motor's modelling:

$$R(\theta) = \begin{pmatrix} \cos(\theta) & -\sin(\theta) \\ \sin(\theta) & \cos(\theta) \end{pmatrix} \tag{6}$$

The third stage of the energy conversion process is the friction between stator and rotor which outputs the torque appearing on the shaft as a function of the wave's amplitude which is then the key variable controlling the motor.

B. Complex phasors.

It's quite common to use complex phasors in Electromagnetic machines with a rotating magnetic flux[9]; they are useful to reach simple representation of electrical variables (voltage or current) of the machine for steady state, and to find out their values. With complex phasors, we focus our attention on RMS or average value of the key variables.

In this section, we are applying concept of complex phasors to TWUM. We look forward a simple representation which help to deduce wave's amplitude as a function of the supply voltage's amplitude and frequency. Complex phasors rely on the concept of *rotating reference frame*. In fact, instant values of w_α and w_β can be deduced from respectively the imaginary part and the real part of a complex number $\underline{w}$. And because w_α and w_β are sinusoidal function of time, the edge of $\underline{w}$ seems to rotate in the complex plane. It's the same for v_α and v_β which can be deduced from $\underline{v}$. This concept of rotating reference frame is summarized in figure 2

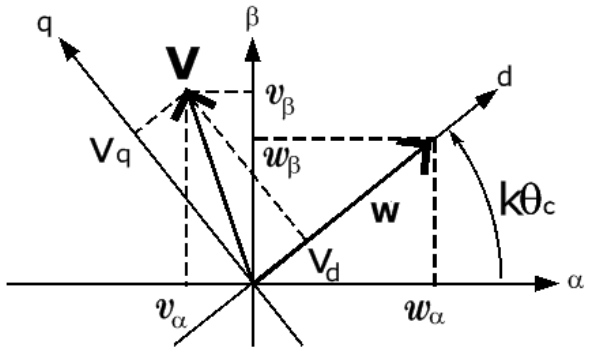

Fig. 2. Instant values of the stationary waves and voltages and the equivalent complex phasor $\underline{w}$ and $\underline{w}$.

For that purpose, we define the following complex variables:

$$\underline{w} = w_\alpha + jw_\beta \tag{7}$$

$$\underline{v} = v_\alpha + jv_\beta \tag{8}$$

At this step, we can deduce from 2 that:

$$\underline{w} = \sqrt{w_\alpha^2 + w_\beta^2}e^{jk\theta_c} \tag{9}$$

and define

$$W = \sqrt{w_\alpha^2 + w_\beta^2} \tag{10}$$

W is the wave's amplitude; 10 leads to:

$$\underline{w} = We^{jk\theta_c} \tag{11}$$

Moreover, defining $\underline{f}_r$, and using 5 and 6 we can write:

$$\underline{f}_r = f_{r\alpha} + jf_{r\beta} = (F_N + jk\frac{h}{b^2}T)e^{jk\theta_c} \tag{12}$$

The relationship between the complex phasors presented in this section is deduced from 3 and 4. In fact, $(3) + j \times (4)$ leads to:

$$m\ddot{\underline{w}} + d_s\dot{\underline{w}} + c\underline{w} = N\underline{v} - \underline{f}_r \tag{13}$$

To calculate the first and second derivatives of $\underline{w}$, we use 11 leading to:

$$\dot{\underline{w}} = \frac{d}{dt}(We^{jk\theta_c}) = \dot{W}e^{jk\theta_c} + jk\dot{\theta}_cWe^{jk\theta_c} \tag{14}$$

When using complex phasors, we consider steady state only. In this condition, $\dot{W}$ is obviously equal to 0, since it's the wave's amplitude of the stator. Moreover, for a perfect travelling wave propagating in the stator, the velocity of the contact point is given by the voltages' frequency ω, and we have $k\dot{\theta}_c = \omega$; ω is supposed to be constant for steady-state operation. Finally, 14 can be revised to take into account steady-state assumption:

$$\dot{\underline{w}} = j\omega We^{j\omega t} \tag{15}$$

Leading to

$$\underline{\ddot{w}} = -\omega^2 W e^{j\omega t} \tag{16}$$

Using 12, 15 and 16 into 13 leads to

$$(-m\omega^2 W + jd_s\omega W + cW)e^{j}\omega t = N\underline{v} - (F_N + jk\frac{h}{b^2}T)e^{j\omega t} \tag{17}$$

In the purpose of simplification, we can lay down

$$\underline{v} = (V_d + jV_q)e^{j\omega t} \tag{18}$$

One will notice that $\sqrt{V_d^2 + V_q^2} = V$, with V voltage's amplitude. Finally, 17 can be revised in:

$$-m\omega^2 W + jd_s\omega W + cW = N(V_d + jV_q) - (F_N + jk\frac{h}{b^2}T) \tag{19}$$

Equation 19 is of prime importance because it helps to find vibration's amplitude of the stator, as a function of external conditions (load torque T and normal preload F_N) as a function of the supply conditions (V and ω). It can be divided into real and imaginary parts, leading to two new equations:

$$(c - m\omega^2)W = NV_d - F_N \tag{20}$$

$$d_s\omega W = NV_q - k\frac{h}{b^2}T \tag{21}$$

This can be summarized on a scheme of figure 3.

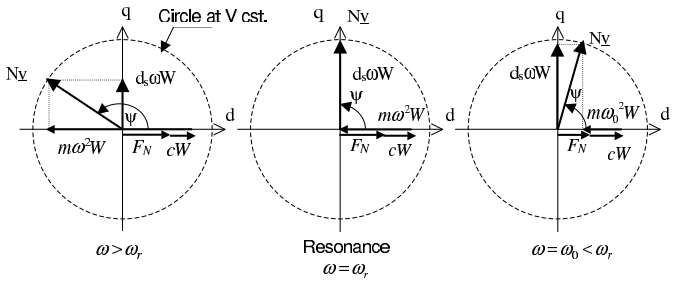

Fig. 3. Vector representation of steady-state operation in the rotating reference frame; T=0.

On this scheme, axis d is the real axis, axis q is the imaginary one. Moreover, we assume that the supply voltages have a constant amplitude (but varying frequency). So the edge of V moves along a circle which radius is V.

For no load conditions ($T = 0$), and according to equation 21, W can be deduced from the projection of phasor $\underline{v}$ on axis q, while V_d satisfies 20. As ω becomes close to the resonant frequency of the motor, V_d decreases and V_q increases: W is thus increasing. The maximum value for W is thus attained if the phasor V is fully projected on axis q. For this operating point $V_d = 0$.

If the motor is supplied below its resonant frequency, the motor stalls. This is well described in [4] and [10]. However, stability of the motor for no load condition is not detailed in this article.

We can measure Ψ, the angle between $\underline{v}$ and $\underline{W}$. One can notice that Ψ decreases as the motor comes close to resonance to reach $\Psi = \frac{\pi}{2}$ for that point.

It is possible to measure Ψ during experiments. In fact, as it is known for complex phasors, the angle measured on a complex plane is also a delay measured on the scope. In the case of TWUM, we have to measure the delay between the supply voltage v_α and w_α (or between v_β and w_β). In this article, we give experimental result obtained with a Shinsei USR60 [11] On the stator of TWUM, a sensor is glued which provides a voltage proportional to stator's deformation named v_{EA}. Unfortunately, the sensor is not at the right place, and an additional delay of 254^o has to be taken into account between sensor's voltage and w_α .

Figure 4 shows records of v_α , v_β and v_{EA} for steady state and $W = 2\mu m$. A phase shift of 98^o is measured, leading to $\Psi = 156^o$ when taking into account the location of the sensor. The corresponding complex phasors are depicted in figure 5.

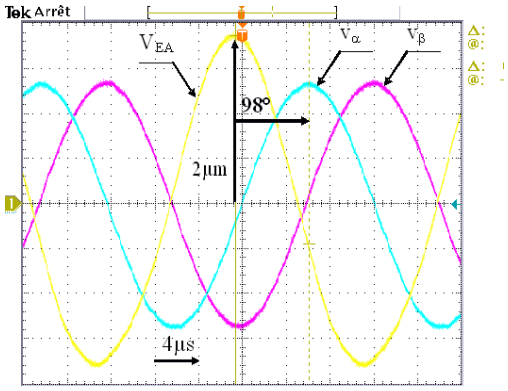

Fig. 4. Records of motor's supply voltages and sensor's output for $W = 2\mu m$.

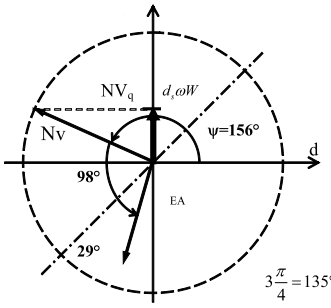

Fig. 5. Complex phasors for $W = 2\mu m$.

Figure 6 presents other records at $3\mu m$. Now, a phase shift of 114^o is measured, leading to $\Psi = 140^o$. These results are consistent with the analysis of figure 3, because Ψ decreases if W decreases. They show that complex phasors are useful to describe motor's operating point. In the next section, we use them to analyze stability of the motor besides external load torque.

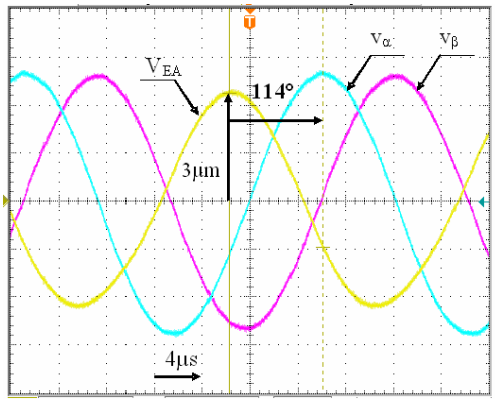

Fig. 6. Records of motor's supply voltages and sensor's output for $W = 3\mu m$.

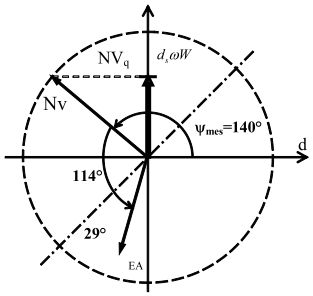

Fig. 7. Complex phasors for $W = 3\mu m$.

III. Stability analysis beside external load torque

A. Effect of a load torque

If a load torque is applied on the shaft as depicted in figure 8, V_q - the projection of $\underline{v}$ on q axis - is divided into two parts: one part for the wave propagation, one part dedicated to the load torque T. For a given wave amplitude W, if the load torque increases, then $\underline{v}$ is coming closer to the q axis.

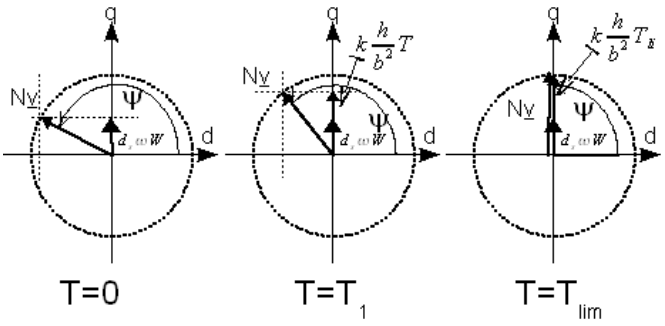

Fig. 8. Vector representation at resonance with two load torque values.

Once again, this can be experimentally verified by records of figure 9. For this run, W is equal to $2\mu m$ as in figure 4, but now, an external load torque of $T = 0.5Nm$ is applied on the shaft. As a consequence, the measured phase shift between v_{EA} and v_α is equal to 120^o, leading to $\Psi = 126^o$: $\underline{v}$ is getting closer to axis q as T increases.

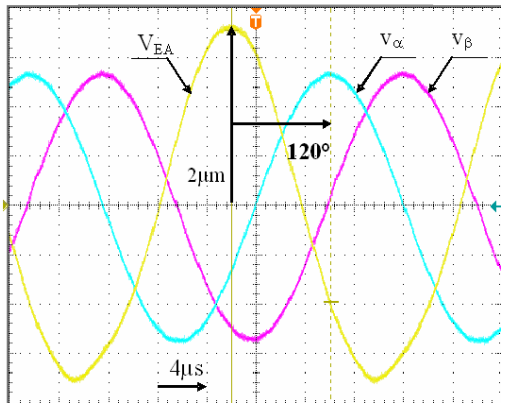

Fig. 9. Records of motor's supply voltages and sensor's output for $W = 2\mu m$ and a load torque $T = 0,5Nm$.

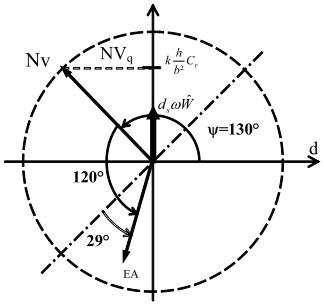

Fig. 10. Complex phasors for $W = 2\mu m$ and $T = 0,5Nm$.

From figure 8, we can deduce that the maximum load torque which allows a stable operation of the motor is then given in the case when $\underline{v}$ is aligned on axis q. At this point, if T becomes larger, the motor stalls, because it is not able to develop a higher torque: equation 21 has no solution. So, stable operations are ensured if

$$\Psi < \frac{\pi}{2} \tag{22}$$

is verifed.

B. Safe operating area.

The safe operating area of a TWUM is a zone delimited by three bounds defined as follows:

- W must be lower than a mechanical limit beyond which the bonding layer would be destroyed. This limit is named W_{Max},
- T can't be larger than a limit defined by tribological contact conditions between stator and rotor. This limit is named T_{Max},
- The motor should not stall. This define a maximum operating torque, named T_{lim}.

T_{lim} is a function of V and W. In fact, starting from equation 21 we can deduce that the maximum available torque is given for $V_q = V$, leading to:

$$k\frac{h}{b^2}T_{lim} = NV - d_s\omega W \tag{23}$$

In figure 11, we have drawn the bounding conditions of the safe operating area in the (T,W) plane, which seems to be more appropriate, for two values of the supply voltage V ($V1 > V2$).

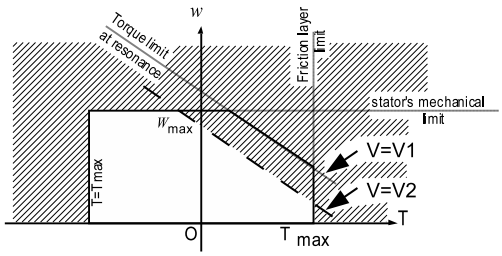

Fig. 11. Safe Operating Area for TWUM in (T,W) plane for $V = V1$ and $V = V2$, $V1 > V2$.

Figure 11 explains why, during operation, the motor may stall if extra load torque is applied on shaft of the motor. The maximum load torque depends on the operating point itself: the bigger W is, the less available torque. Moreover, We also understand why increasing motor's voltage is a solution to the problem: in fact, this increases the maximum available torque for each travelling wave's amplitude. However, this solution is not effective because it is leading to additional power losses in the motor and heat.

C. Experimental measurement of the safe operating area.

It is possible to measure T_{lim} as a function of W and V. For that purpose, we increase the load torque on the shaft, by using a powder brake for example, and ω is adjusted so as to keep W constant. During this test, we also measure the phase shift between v_α and v_{EA}, so as to estimate Ψ. All the variables are recorded. We note the value of T and Ψ when the motor suddenly stalls (W falls down to zero then) while it was rotating normally just before. Runs of figure 12

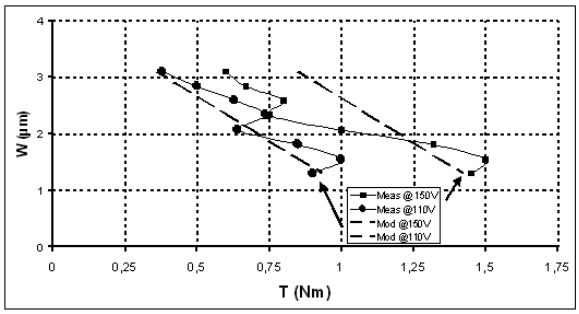

Fig. 12. Safe Operating Area for a Shinsei USR60 at $V = 150V$ and $V = 110V$.

show that the maximum available torque T_{lim} really depends on W and V. However, we have found curves which are not equal to the modelling presented in this article. Of course, errors can be due to measurement errors of the load torque, or to the protocol (it's difficult to exactly know whether the motor is stall or not). But it may also be due to the modelling which is not accurately taking into account the specific contact conditions between stator and rotor.

Moreover, we do not verify in figure 13 that $\Psi = \frac{\pi}{2}$ when the motor stalls; at the moment, we can't find a reason why such a difference occurs.

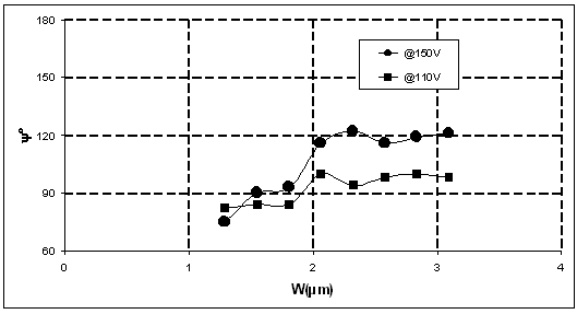

Fig. 13. value of Ψ when the motor stalls for $V = 150V$ and $V = 110V$.

However, because Ψ can be easily measured on the motor, while measuring the load torque can't be expected in our application, keeping $\Psi > 120^o$ is a good solution for avoiding stalling of the motor at any voltage. This method will be exploited in a control detailed in the next section

IV. Wave amplitude controls of TWUM.

In TWUM, the key variable controlling torque and speed of the motor is W. This is why we should always find a Wave amplitude control loop in control schemes of TWUM. This section describes classical and new control strategies.

A. Frequency control

In classical control, the frequency ω of the supply voltages is controlled so as to obtain a reference value of W, as shown in figure 14. This frequency control is straightforward, but is also very sensitive to the external conditions. In this control, W is set independently of the load torque, and if a load larger than T_{lim} is applied, the motor stalls. To start up again, a long and specific procedure has to be followed: closed loop control fails. In order to increase the torque limit, increasing V is useful, but does not completely remove the problem. Moreover, it's difficult to precisely tune the loop controler, because the relationship between W and ω is not linear. But this control is made of a single loop, leading to excellent performances in term of response time.

B. Control in a rotating reference frame

In addition to voltage's increase, we could adapt the reference value W_{ref} of figure 14 in case of large load torque as described in figure 11: from the measurement of T, W is adapted so as to ensure stable operation at resonance.

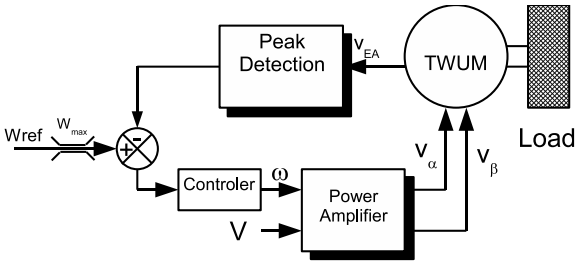

Fig. 14. Frequency control of a TWUM.

However, this solution is difficult since the measurement of T requires space, weight and cost.This is why, instead of measuring T, it is better to measure Ψ[4][12]; stable operation of the TWUM above the resonant frequency will be ensured if 22 is verified. So [4] advises to control Ψ by an internal loop as shown in figure 15. This increases reliability, but at the expense of a time delay for the control of W due to the internal loop of Ψ. This is why, a hybrid control is proposed, which takes benefit from both control strategies.

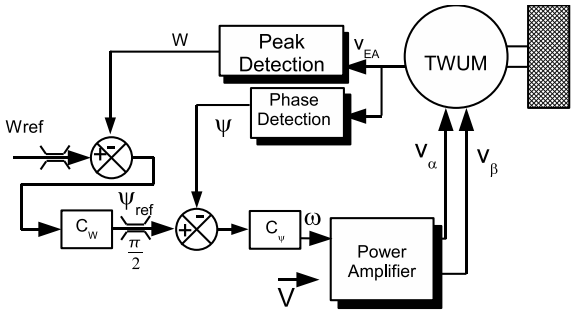

Fig. 15. Control in a rotating reference frame.

C. Hybrid control strategy

This control depicted on figure 16 uses two controllers running in the same time. One is using a frequency controller C_W to control W to the reference W_{ref}. The other is using the controller in the rotating reference frame C_Ψ to control $\Psi = \frac{\pi}{2}$. A strategy block switches from one controller to the other, depending on their output.

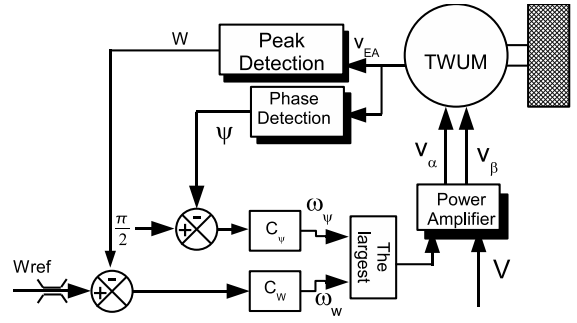

Fig. 16. Proposed strategy.

Under normal operating conditions, the motor is far from its resonance. So ω_W is larger than ω_Ψ . The motor is then frequency controlled (point (1) in figure 17). If T increases, Ψ decreases because V_q is becoming larger according to section III. At point (2), $\omega_W = \omega_\Psi$ because $W = Wref$ and $\Psi = \frac{\pi}{2}$. For a larger load torque, W_{ref} cannot be attained; the frequency controller fails to control W; at In this mode $\omega_W < \omega_\Psi$, so Ψ is controlled. Consequently, W automatically adapts to the load torque: performances are diminished, but the motor doesn't stall.

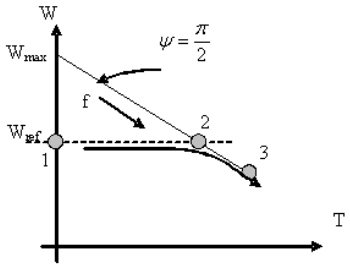

Fig. 17. W as a function of T with hybrid control.

D. Experimental runs

The hybrid control is checked during experimental runs. The TWUM used is a Shinsei USR60, driven by a linear power amplifier. A specific control electronic has been built and can be used for controlling the motor in its rotating reference frame; details can be found in[4]. An inertial load ($10^{-4} kgm^2$) is attached to the shaft and a powder brake as well (figure 18). Moreover, the position of the motor is controlled as detailed in[13][2]. The required performances are $200ms$ response time, $1,3mrad$ of position error (5000 dots/rev). During the experiment, Ψ_{ref} is not equal to $\frac{\pi}{2}$ but 120^o as shown in section III. We use Dspace 1104 board to implement control rules.

Fig. 18. the experimental test bench.

During the first run depicted on figure 19, the powder brake is off. Only load inertia is applying torque on the shaft. This is

the normal operating mode: the measured value of Ψ is larger than the reference, the motor is fully frequency controlled. For

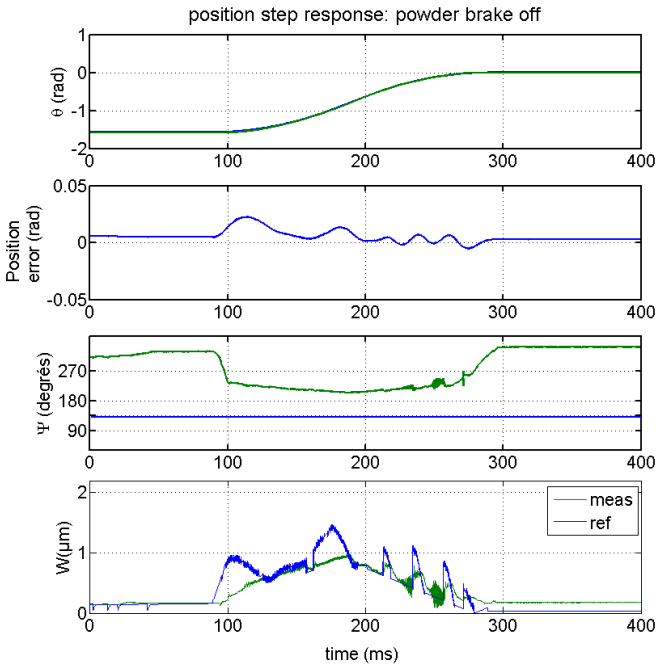

Fig. 19. position step response when powder brake off @150V.

the second run of figure 20, an additional load torque is applied thanks to the powder brake. Because this additional torque is too large, W has to be reduced compared to its reference. This is automatically achieved by using the proposed method. In fact, the motor operates close to its resonance, without stalling, and provides then its better performances for this load condition. Of course, time response is increased, but reliability is ensured.

V. Conclusion

In this paper, we present a novel control method which increases reliability of servo mechanism using TWUM. This method is a hybrid control between a classical frequency control and a control in a rotating reference frame. Experimental results confirm performances at low supply voltage level. Moreover, the strategy is included in a position control loop.

References

[1] T.Senjyu, T.Kashiwagi and K. Uezato, "Position control of ultrasonic motors using mrac and dead-zone compensation with fuzzy inference," *IEEE Transactions on Power Electronics*, vol. 17, pp. 265–2729, Mar. 2002.

[2] F.Giraud, B.Semail, J.Aragones, J.Robineau and J.-T.Audren, "Precise position control of a travelling wave ultrasonic motor," *Proceeding of the 40th IAS annual meeting – Hong-Kong*, vol. 3, pp. 1548–1554, Oct. 2005.

[3] J.Maas, T. Schulte, H.Grostollen, "Optimized drive control for inverter-fed ultrasonic motors," *IEEE Industry applications society (IAS'97)*, vol. 1, pp. 690–698, Oct. 1997.

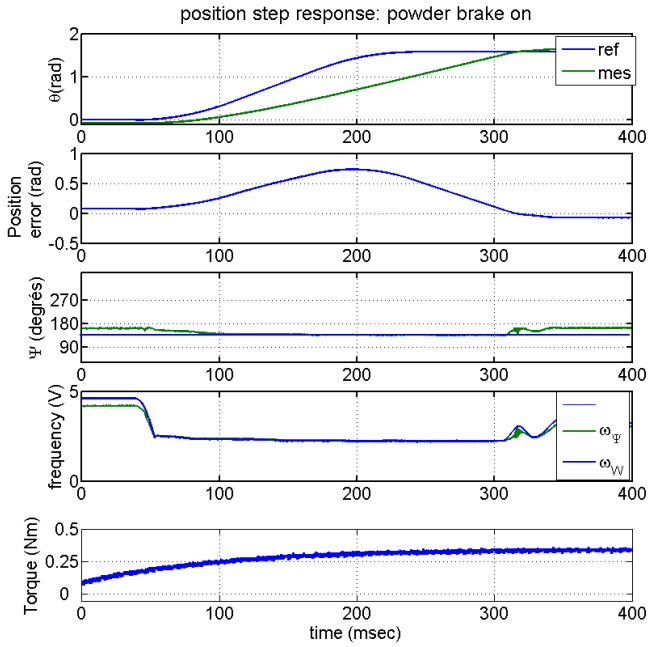

Fig. 20. position step response when powder brake on @150V.

[4] F. Giraud, B. Semail, and J.-T. Audren, "Analysis and phase control of a piezo electric travelling wave ultrasonic motor for haptic stick application," *IEEE trans. on Industry applications*, vol. 40, pp. 1541–1549, nov-dec 2004.

[5] W. Hagood IV, A.J. McFarland, "Modeling of a piezoelectric rotary ultrasonic motor," *IEEE Transactions on ultrasonics, ferroelectrics and frequency control*, vol. 42, no. 2, Mar. 1995.

[6] N. E. ghouty, "Hybrid modeling of a traveling wave piezo electric motor," Ph.D. dissertation, Aalborg University, department of control engineering, May 2000.

[7] F.Giraud, B.Lemaire-Semail, "Causal modeling and identification of a traveling wave ultrasonic motor," *The European Physical Journal of Applied Physics*, no. 2, Feb. 2003.

[8] B.-S. F.Giraud, "A torque estimator for a traveling wave ultrasonic motor - application to an active claw," *IEEE Transactions on Ultrasonics, Ferroelectrics and Frequency Control*, vol. 53, pp. 1468–1477, Aug. 2006.

[9] P.Vas, *Vector control of AC machines*. Oxford Science Publications, 1990, iSBN 0-19-859370-8.

[10] J.Maas, T. Schulte, H.Grostollen, "Controlled ultrasonic motor for servo-drive applications," *4th Eur. Conf. on smart structures and materials, 2nd Int. Conf. on micromechanics, intelligent materials and robotics (MIMR'98)*, pp. 701–708, 1998.

[11] Shinsei corporation, "Internet website," http://www.shinsei-motor.com.

[12] M.Budinger, F.Giraud, B.Nogarède, J.-F. Rouchon, B.Lemaire-Semail, "Feeding and control electronic of a piezoelectric actuator," *8th Int. Conf. on new actuator (ACTUATOR 98)*, pp. 363–366, Jun. 2002.

[13] F.Giraud, B.Semail, "Position control of a small travelling wave ultrasonic motor," *Proceeding of the International Conference on New Actuators – ACTUATOR'2004*, Jun. 2004.